Characterizing the membrane properties of capsules flowing in a square-section microfluidic channel: Effects of the membrane constitutive law

X.-Q. Hu, B. Sévénié, A.-V. Salsac,* E. Leclerc, and D. Barthès-Biesel
Laboratoire de Biomécanique et Bioingénierie (UMR CNRS 7338), Université de Technologie de Compiègne, CS 60319, 60203 Compiègne, France
(Received 19 February 2013; published 13 June 2013)

A microfluidic method is presented to measure the elastic membrane properties of a population of microcapsules with diameter of order 60 μm. The technique consists of flowing a suspension of capsules enclosed by a polymerized ovalbumin membrane through a square-section microfluidic channel with cross dimension comparable with the capsule mean diameter. The deformed profile and the velocity of a given capsule are recorded. A full mechanical model of the motion and deformation of an initially spherical capsule flowing inside a square-section channel is designed for different flow strengths, confinement ratios, and membrane constitutive laws. The experimental deformed profiles are analyzed with the numerical model. This allows us to find the ratio between the viscous and elastic forces and thus the shear elastic modulus of the membrane. We show that the ovalbumin membrane tends to have a strain-softening behavior under the conditions studied here.

DOI: 10.1103/PhysRevE.87.063008 PACS number(s): 47.63.−b, 87.16.D−, 46.15.−x

I. INTRODUCTION

Capsules, which are liquid droplets enclosed by a thin elastic membrane, are widely found in nature (red blood cells, eggs) and in cosmetic, food, or pharmaceutical industry [1]. The deformable membrane that separates the internal and external liquids prevents the diffusion and degradation of the internal substance and controls its release. The motion and deformation of flowing capsules depend on the mechanical properties of the membrane. The characterization of these properties is thus essential for the design of artificial capsules, but it is a challenging task when the capsules have a small size of order a few tens of micrometers. Artificial capsules are usually obtained through interfacial polymerization of a liquid droplet and are thus spherical. In the following, we consider only initially spherical artificial capsules with radius a.

A method that is widely used for relatively large millimeter-size capsules is to compress them between two rigid parallel plates and measure simultaneously the plate separation and compression force. Using an appropriate mechanical model of the setup, the membrane constitutive law can be deduced [2]. Subjecting capsules to simple shear flow [3] or to centrifugal flow fields [4] are two other possible ways to measure the membrane properties. However, it is difficult to reach large mechanical stresses in such devices.

For micrometer-size capsules, poking the membrane with an atomic force microscope [5] or sucking part of it in a micropipette [6,7] are classical techniques to measure the membrane mechanical properties. Both require skillful micromanipulations and are not suitable for screening large populations of microcapsules quickly. Recently a new method has been proposed to measure the membrane properties of a capsule population. It consists of flowing a capsule suspension into a cylindrical glass capillary tube with radius comparable to that of the capsules [8,9]. Hydrodynamic forces and boundary confinement lead to a large deformation of the capsules, which can take either a parachute or a slug shape. The membrane mechanical properties are then determined by analyzing the experimental results with a numerical model of the setup. This method, applied to 62 μm mean diameter capsules with a cross-linked ovalbumin membrane, allows one to correlate the membrane mechanical properties to the cross-linking degree and to the physicochemical conditions of the capsule fabrication [9]. It is, however, not easy to connect the syringe pump to the 50 μm diameter capillary tube, where the measurement is performed. A double tube was designed, but it leads to fairly large pressure drops.

The rapidly growing microfluidic technologies allow one to design simpler devices, in which the capillary tubes are easily connected to the feeding system. Owing to fabrication constraints, the tubes usually have a square or rectangular cross section. We thus investigate the feasibility of using a microfluidic channel with a square cross section to measure the membrane properties of a population of capsules suspended in a viscous fluid. The channel has a side length 2ℓ of the same order of magnitude as the capsule mean diameter $2a$. We will see that the initially spherical capsule can be subjected to significant deformations depending on the flow velocity and size ratio a/ℓ between the capsule and the channel. This means that it will be possible to discriminate which type of constitutive law the membrane follows.

The analysis of the experiments requires a specific numerical model of the flow of a capsule in a square pore. Kuriakose and Dimitrakopoulos [10] recently designed such a model, based on the use of spectral elements, for capsules composed of a strain-hardening membrane described by a Skalak *et al.* law [11]. However, the capsules had to be pre-inflated and thus prestressed in order to prevent buckling instabilities. If the prestress has a negligible influence when the capsule is highly deformed, it changes the results significantly at small and moderate deformation [12]. We use instead the three-dimensional fluid-structure interaction scheme initially proposed for capsules freely suspended in unbounded flows [13] and recently adapted for capsules flowing in circular and square-section channels [14]. This numerical technique consists of coupling the boundary integral method for the

*a.salsac@utc.fr

fluid flows with a finite element method for the membrane deformation. The advantages of this model are twofold: the capsules do not need to be prestressed, and large confinement ratios can be considered. In Hu *et al.* [14], we have studied in detail the case of capsules with a strain-softening neo-Hookean membrane. We now extend the results to the case of capsules with a strain-hardening law in order to analyze the experimental results with either law.

We first present the experimental method used to measure the deformation of artificial capsules flowing in a square-section capillary tube. We then explain briefly the mechanical model that represents the experiments, and we give global results on the capsule deformation and kinematics as functions of the suspending flow strength and confinement. Finally we show how the method can be used to estimate the shear elastic modulus of the membrane of a capsule population and discuss the limits of the method.

II. MATERIALS AND METHODS

A. Capsule fabrication

Microcapsules are prepared using an interfacial cross-linking method [15]. Briefly, a 10% (w/v) ovalbumin (Sigma) solution is prepared using a phosphate buffer with pH = 5. The solution is emulsified in cyclohexane (SDF) containing 2% (w/v) sorbitan trioleate (Sigma) at a stirring speed of 1550 rpm. A 2.5% (w/v) solution of terephthaloyl chloride (Acros) in chloroform:cyclohexane (1:4 v/v) is then added to the emulsion, and the cross-linking reaction is allowed to develop for 5 min. The reaction is stopped by diluting the reaction medium with cyclohexane. The microcapsules are separated from the organic phase by centrifugation and washed successively with cyclohexane, with water containing 2% (w/v) polysorbate (Sigma) and finally washed three times with pure water in which the samples are kept. The resulting capsules have a mean diameter of 62 ± 14 μm.

B. Microfluidic system fabrication

Straight 5-mm-long square-section channels are fabricated by molding liquid polydimethylsiloxane onto a silicon master and baking and peeling it off [16,17]. The channels are then closed bonding them onto a glass lamella by air plasma (Plasma cleaner, Harrick). The width of the channel is estimated to be $W = 57.5 \pm 1.5$ μm using a line graduated rule to estimate the pixel to μm conversion factor. The depth of the channel, measured on the silicon mold, is $h = 52 \pm 1$ μm. As the channel cross section is not perfectly square, we define the length 2ℓ as the side of the ideal square cross section channel having the same cross-area:

$$\ell = \frac{\sqrt{Wh}}{2} = 27.4 \pm 0.5\,\mu\text{m}. \quad (1)$$

C. Capsule suspension preparation

A volume of 40 μl of ovalbumin microcapsule sediment is suspended in 1.8 ml of glycerin (100%, VWR BDH Prolabo), which leads to a 2.2% (w/v) capsule suspension. After mixing by successive pumping in and out of a syringe, the suspension is left to rest for 10 min at a room temperature of 23 °C to allow the inner water to be replaced by the outer glycerin by osmotic exchange. This process does not seem to damage the capsules, which recover a spherical shape within minutes. As a consequence, we consider that there is no osmotic difference between the internal and external liquids and that the membrane is thus not prestressed. The viscosity μ of the suspending fluid strongly depends on temperature and water content [18]. Former measurements of the suspension [9] provided a viscosity of $\mu = 0.7$ Pa s at 23 °C. We assume this value to be the viscosity of the fluid carrier and thus neglect the influence of the small amount of capsules present in the suspension.

D. Experimental setup

We fill a 1 ml glass syringe (Fortuna Optima) with the suspension and take care that no air bubble remains in either the syringe or the silicon connection tube to minimize throughput variations. The suspension is injected into the microfluidic system by means of a syringe pump (KDS100, KD Scientific) at different flow rates. The deformation and velocity of a capsule is observed with a ×40 magnification transmission microscope (Leica DM IL LED), which is connected to a high-resolution high-speed camera (FASTCAM SA3 Photron) through a ×1 C-mount (Leica). The microscope is focused on the channel center plane. The capsule profile is observed along the channel axis and width W. The images are recorded at 1000 frames per second, with an exposure time of 0.2 ms and an observation field 1024 × 256 pixels. The calibration scale is 0.425 μm/pixel. The observation field is far enough from the entrance (about 3 mm, i.e., 100ℓ) to consider that the capsule has reached a steady state. From two successive images, we measure the capsule velocity v_o, which varies between 1 and 10 mm/s, depending on the size of the capsule and the flow rate.

E. Capsule profile extraction and experimental measurements

Figure 1(a) shows an experimental image of a capsule flowing in a 2ℓ square channel. Because automatic image extraction is difficult with this low contrast level, we use ImageJ to detect manually the capsule contour. The channel and membrane contours are determined at the center of the dark line. We then calculate the surface S of the profile, its total length L, and its axial length L_a as shown in Fig. 1(b). The parachute depth is given by $L_p = L - L_a$. The experimental error on the lengths 2ℓ, L, L_a is of order 1 μm. The wall corrugations, which appear in Fig. 1(a), are also of order

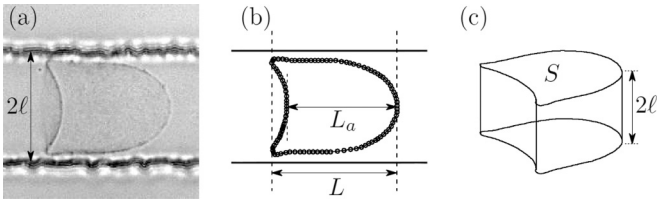

FIG. 1. Capsule profile extraction from an experimental image: (a) initial image; (b) contour extracted with ImageJ; (c) approximate capsule volume based on the contour area and channel depth.

1 μm. They lead to small oscillations of the capsule profile, which are of the same order as the measurement error.

The initial capsule radius a cannot be inferred directly from the experimental images, which are only projections of the deformed profile. We thus estimate an approximate capsule volume as the volume of a cylinder with section S and height 2ℓ [Fig. 1(c)]. This allows us to calculate an approximate capsule radius $a_{\rm app}$ given by

$$a_{\rm app} = \left(\frac{3\ell S}{2\pi}\right)^{1/3}. \tag{2}$$

The relationship between $a_{\rm app}$ and the exact radius a is given by the numerical model of the capsule flow problem.

III. MODEL OF THE FLOW OF A CAPSULE IN A PORE

In order to analyze the experiments, a mechanical model of the set-up is needed. The flow of a capsule in circular [12,19] or square [10,14] cross-sectional channels has been studied. We briefly outline the numerical model and provide new results for the flow of capsules in square-section channels for a wide range of size ratios and flow strengths, for strain-hardening or strain-softening capsule membranes. Details on the problem equations and their solution by means of the coupled boundary integral and finite element methods can be found in Hu *et al.* [14].

A. Problem statement

An initially spherical capsule (radius a) flows along the z axis of a microfluidic channel with a square cross section (side 2ℓ) in the perpendicular xy plane. The interior and exterior of the capsule are incompressible Newtonian fluids with the same density ρ and viscosity μ. The thin membrane of the capsule is an impermeable hyperelastic isotropic material with surface shear modulus G_s and area dilatation modulus K_s. Apart from the capsule membrane mechanical properties, the two other main parameters of the problem are the size ratio a/ℓ between the capsule initial radius and the channel cross dimension, and the capillary number

$$\mathrm{Ca} = \mu V/G_s, \tag{3}$$

which measures the ratio between viscous and elastic forces, where V is the mean external undisturbed flow velocity along the z axis of the channel.

We denote $\boldsymbol{v}^{(\beta)}$, $\boldsymbol{\sigma}^{(\beta)}$, and $p^{(\beta)}$ the velocity, stress, and pressure fields in the suspending ($\beta = 1$) and internal ($\beta = 2$) liquids. The flow Reynolds number is assumed to be very small, so that the internal and external liquid motions satisfy the Stokes equations:

$$\nabla p^{(\beta)} = \mu\nabla^2\boldsymbol{v}^{(\beta)}, \quad \nabla\cdot\boldsymbol{v}^{(\beta)} = 0, \quad \beta = 1,2. \tag{4}$$

They are solved in a domain bounded by the cross sections S_1 at the tube entrance and S_2 at the exit, both located far from the capsule center of mass (Fig. 2). The other domain boundaries are the channel wall W and the capsule surface C. The unit normal vector $\boldsymbol{n}$ to all the boundaries points towards the suspending liquid. The problem boundary conditions are:

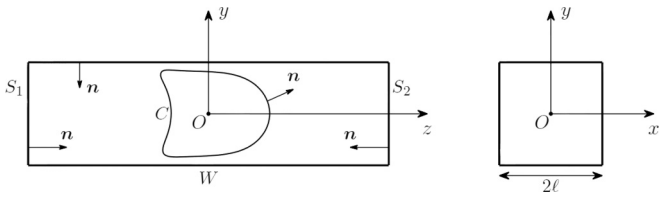

FIG. 2. Prismatic channel with axis Oz. The cross section is square with side 2ℓ.

(1) No flow disturbance on S_1 and S_2 as they are far from the capsule:

$$\boldsymbol{v}^{(1)}(\boldsymbol{x},t) \to \boldsymbol{v}^{\infty}(\boldsymbol{x}), \quad \boldsymbol{x}\in S_1\cup S_2, \tag{5}$$

where $\boldsymbol{v}^{\infty}$ is the flow velocity in a square channel in the absence of capsule.

(2) Uniform pressure on S_1 and S_2:

$$p^{(1)}(\boldsymbol{x},t) = 0 \quad \boldsymbol{x}\in S_1, \tag{6}$$

$$p^{(1)}(\boldsymbol{x},t) = \Delta P(t) + \Delta P^{\infty} \quad \boldsymbol{x}\in S_2, \tag{7}$$

where ΔP^{∞} is the undisturbed pressure drop between S_1 and S_2 in the absence of capsule and ΔP is the additional pressure drop due to the capsule.

(3) No slip on the channel wall W:

$$\boldsymbol{v}^{(1)}(\boldsymbol{x},t) = \boldsymbol{0}, \quad \boldsymbol{x}\in W. \tag{8}$$

(4) No slip on the capsule-deformed surface C:

$$\boldsymbol{v}^{(1)}(\boldsymbol{x},t) = \boldsymbol{v}^{(2)}(\boldsymbol{x},t) = \frac{\partial}{\partial t}\boldsymbol{x}(\boldsymbol{X},t), \quad \boldsymbol{x}\in C, \tag{9}$$

where $\boldsymbol{X}$ denotes the initial position of a membrane material point located at position $\boldsymbol{x}$ at time t.

(5) The load per unit area $\boldsymbol{q}$ on the membrane is due to the viscous traction jump:

$$(\boldsymbol{\sigma}^{(1)} - \boldsymbol{\sigma}^{(2)})\cdot\boldsymbol{n} = \boldsymbol{q}, \quad \boldsymbol{x}\in C. \tag{10}$$

B. Membrane laws

As the membrane thickness is negligibly small compared to the capsule dimensions, the membrane can be treated as a hyperelastic surface devoid of bending stiffness. The in-plane deformation is then measured by the principal extension ratios λ_1 and λ_2. Owing to the combined effects of hydrodynamic forces, boundary confinement, and membrane deformability, the capsule can be highly deformed as shown in Fig. 1. Consequently the choice of the membrane constitutive law is important. We consider two simple laws with constant material coefficients. One such law (NH) is the widely used neo-Hookean law, which models the membrane as an infinitely thin sheet of a three-dimensional isotropic and incompressible material. The principal Cauchy in-plane tensions (forces per unit arc length of deformed surface curves) can be expressed as [20]

$$\tau_1 = \frac{G_s}{\lambda_1\lambda_2}\left[\lambda_1^2 - \frac{1}{(\lambda_1\lambda_2)^2}\right] \text{ (likewise for } \tau_2). \tag{11}$$

The membrane dilatation modulus K_s is then given by $K_s = 3G_s$.

Another law was originally proposed by Skalak *et al.* [11] to describe the membrane deformations of red blood cells. The principal tensions are

$$\tau_1 = \frac{G_s}{\lambda_1\lambda_2}\left[\lambda_1^2\left(\lambda_1^2-1\right)+C\left(\lambda_1^2\lambda_2^2\right)\left(\lambda_1^2\lambda_2^2-1\right)\right] \quad \text{(likewise for } \tau_2\text{)}, \tag{12}$$

where the dimensionless parameter C mainly measures the resistance to area dilatation. The membrane dilatation modulus is given by $K_s = (1+2C)G_s$. This law has strain-hardening properties that increase with C for $C \geqslant 0$ [20]. When $C = 1$, the Skalak *et al.* law (SK) and the NH law lead to the same small deformation behavior with the same values of G_s and K_s. Contrary to the SK law, the NH law is strain-softening under large deformation [20]. We thus study the effect of the membrane strain-hardening or -softening property on the capsule deformation by considering the flow of capsules enclosed by either an NH membrane or an SK membrane.

To close the problem, we must relate the load on the membrane given by Eq. (10) to the elastic Cauchy tension tensor $\boldsymbol{\tau}$. In absence of inertia, the membrane equilibrium leads to

$$\nabla_s \cdot \boldsymbol{\tau} + \boldsymbol{q} = \mathbf{0}. \tag{13}$$

C. Numerical procedure

The problem is solved coupling a boundary integral method to solve for the fluid flow and a finite element method to solve for the membrane mechanics [13,14]. The advantage of the procedure is that only the boundaries of the flow domain S_1, S_2, W, C are discretized.

The capsule mesh is generated by first inscribing an icosahedron (regular polyhedron with 20 triangular faces) in the sphere and subdividing the elements sequentially until the required number of elements is reached [13,14]. The capsule mesh is composed of 1280 P_2 elements and 2562 nodes. The mesh of the external boundaries (S_2 and W) is generated using P_1 elements with Modulef (INRIA Rocquencourt, France) [14] and is refined in the central portion of the channel, where the capsule is located. The boundary mesh has 1905 nodes and 3768 elements. All the results are obtained with a nondimensional time step $\Delta t V/\ell = 5\times10^{-5}$.

The equations are solved in a reference frame moving with the capsule center of mass. Thus for each time step, we compute the velocity v_o of the capsule center of mass and move back the whole capsule by $v_o\Delta t/\ell$, so that the capsule remains centered in the tube domain.

The model inputs are the capillary number Ca, the size ratio a/ℓ and the membrane law. The model outputs are the capsule centroid velocity v_o and the steady deformed capsule shape. From the latter, it is possible to compute the evolution of the total length L, of the parachute depth L_p and of the apparent capsule radius a_{app} with size ratio a/ℓ and Ca. The model also yields the elastic tension distribution in the membrane. If a failure criterion is known for the membrane, it is then possible to infer whether there is a risk of breakup.

Since the bending modulus of the membrane has been neglected, the capsule wall buckles locally in the regions where the elastic tensions are compressive [14]. In order to study the postbuckling behavior of the capsule, bending moments and transverse shear forces should be added to Eq. (13) and a constitutive equation should be postulated to relate bending moments and local deformations. It follows that the bending behavior of a capsule is a complicated problem of shell mechanics that is not completely resolved yet. The simplified membrane model that we use here is appropriate to model capsules with a very low bending resistance. It detects zones where tensions are compressive and where the capsule wall may buckle. The use of triangular finite elements allows for some profile oscillations in compression areas without creating any numerical instability. Such numerical "folds" have a wavelength that depends on the grid point spacing. Hence they do not model the physical postbuckling behavior of the capsule [14].

D. Effect of membrane law on capsule deformation

We consider the flow of capsules with an NH or an SK membrane in a microfluidic pore for different size ratios a/ℓ at various flow strengths Ca. It is assumed that the steady-state configuration is reached, when the area of the capsule varies by less than $5\times10^{-4}\,(4\pi a^2)$ over a nondimensional time $Vt/\ell = 1$. All the following results pertain to this equilibrium state. At steady state, the membrane and thus the internal fluid are motionless. This means that assuming the same value of viscosity for the internal and external liquids does not limit the validity of the results; the viscosity ratio influences only the time the capsule needs to reach a steady state (this time increases as the internal viscosity increases). Furthermore, as the pressure inside the capsule is uniform, the curvature at the capsule upstream tip must be larger than at the rear to account for the viscous pressure drop in the lubrication film around the capsule. This explains why parachute or slug shapes are obtained.

We first show the deformed profiles of a large capsule ($a/\ell = 1.1$) in Fig. 3(a) for increasing flow strengths Ca = 0.01, 0.05, 0.07. The axial profile in the zy plane is what is observed experimentally. At low flow strength (Ca = 0.01), the profiles of the NH and SK capsules are almost superimposed, since the two membrane laws are equivalent at small deformations. For Ca = 0.05, a parachute shape is found for the NH capsule, while the SK capsule still has a slug shape. This indicates that the flow strength level Ca_c, for which the parachute shape appears, depends on the membrane constitutive law. The cross-profiles in the xy plane show that the capsule shape is not axisymmetric as the membrane tends to fill the corners of the channel.

Figure 3(b) shows the capsule profile at a high flow strength Ca = 0.1 for various size ratios. The parachute shape appears for all the capsules. The NH capsule is more deformed than the SK one, even though the difference is quite small for small capsules ($a/\ell \leqslant 0.9$). For $a/\ell = 1.10$, we can get a steady-state solution for the SK membrane only. Indeed, a strain-softening NH capsule undergoes continuous elongation, when a maximum flow strength Ca_{max} is exceeded. This phenomenon was already observed in a cylindrical tube where the situation is axisymmetric [9]. It is due to the fact that a strain-softening membrane has a deformation, which increases faster than linearly with the imposed load [1]. The values of

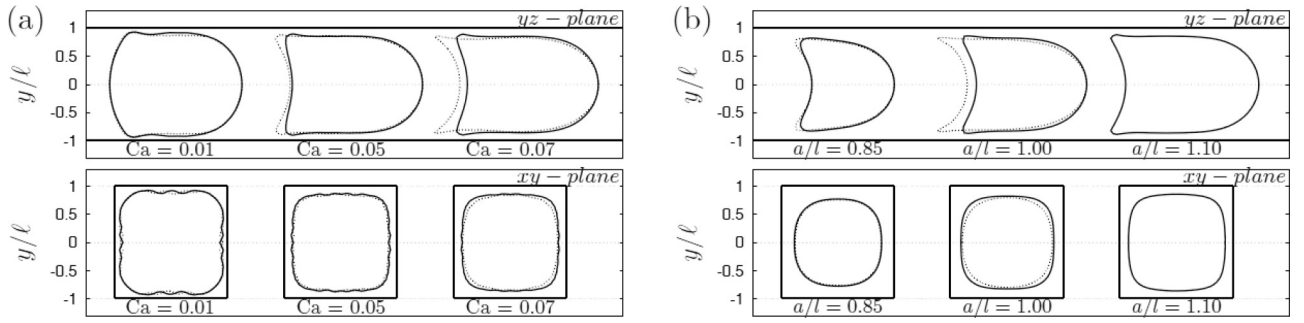

FIG. 3. Comparison of steady profiles (solid line: SK law, dashed line: NH law): (a) effect of Ca for constant $a/\ell = 1.1$; (b) effect of a/ℓ for constant Ca = 0.1.

Ca_{max} for a square-section tube are shown in Fig. 4, where they are compared with the values obtained for a cylindrical tube with radius ℓ. We note that Ca_{max} is slightly larger for a square than for a circular pore because, for the same flow rate, the viscous shear on the capsule is less in a square pore than in a circular one due to the presence of corners. This continuous elongation phenomenon does not occur with an SK membrane, as it is strain-hardening [1].

The overall capsule deformation is quantified by the maximum length L/ℓ and the parachute depth L_p/ℓ, as shown in Fig. 5. The parachute forms at the capsule rear, when the capillary number exceeds the critical value Ca_c. The value of Ca_c is less for an NH capsule than for an SK one. Below Ca_c, the capsule elongation is small and there is little influence of the membrane law. When $Ca > Ca_c$, both L/ℓ and L_p/ℓ increase much faster with Ca for an NH capsule than for an SK one. This is due again to the strain-softening property of the NH membrane, which allows larger deformation for the same stress level than a strain-hardening SK membrane. The overall effect of the size ratio is to increase the deformation for a given flow strength. Finally, we note that the capsule velocity decreases, when the confinement increases or when the deformation decreases.

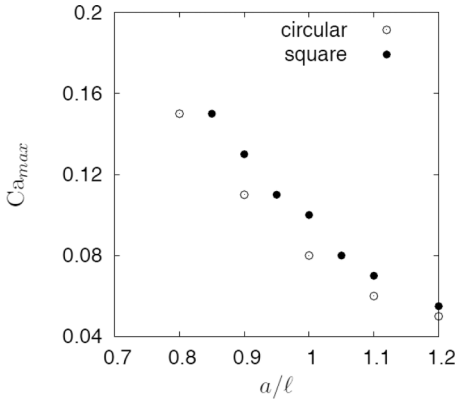

FIG. 4. Maximum values of Ca, for which a steady profile is obtained for a capsule enclosed by an NH membrane. The comparison between a square or circular pore with radius ℓ shows the effect of the corners.

E. Size, deformation, and velocity charts for a capsule with NH or SK law

The results of the numerical model are gathered in charts, where the main output parameters, i.e., total length L/ℓ, parachute depth L_p/ℓ, approximate radius a_{app}/ℓ, and centroid velocity v_o/V, are plotted as functions of Ca and a/ℓ for capsules with an NH membrane (Fig. 6) or with an SK membrane with $C = 1$ (Fig. 7). For the NH capsules, the range of Ca is limited by the continuous elongation phenomenon. For the SK capsules, the range of Ca is a priori unlimited. However, we give results for Ca up to 0.5, because the variation of the different geometrical quantities is almost linear with Ca when $Ca \geqslant 0.2$, while the velocity is almost constant. For very large capsules ($a/\ell \geqslant 1.2$) and high flow strength ($Ca \geqslant 0.5$) the deformation at the rear and the concomitant curvature of the tip become too large to be modeled correctly by a membrane law where bending rigidity is neglected. This is why we do not give results for $Ca > 0.3$ when $a/\ell = 1.2$.

Note that a_{app}/ℓ does not vary much with Ca, except for very low values of Ca. This point will be important for the determination of the actual size ratio of a capsule from the measurement of a_{app}/ℓ. The relative difference between a_{app} and a is of order 17% for small capsules and decreases to less than 10% for the largest capsules. Finally, we have refrained from giving results for small capsules with $a/\ell < 0.85$ because they require high values of Ca to be significantly deformed. Experimentally, such high values of Ca imply high values of the flow velocity V, for which it is difficult to obtain capsules images with good enough contrast and sharpness.

F. Inverse analysis of the experimental results

We have developed a new MatLab program, inspired from the algorithm of Chu *et al.* [9], to automatically perform the inverse analysis of capsule profiles in square channels. The numerical data shown in Figs. 6 and 7 are linearly interpolated on a regular grid. A membrane law is first assumed and the algorithm then determines the size ratio a/ℓ and the capillary number Ca, for which the experimental and numerical values of L/ℓ and L_p/ℓ fit best.

Tolerances have been defined to account for the uncertainty on experimental measurements. Depending on the flow conditions, the membrane can appear more or less fuzzy. Considering an error of 2% on ℓ and L, we assume a tolerance

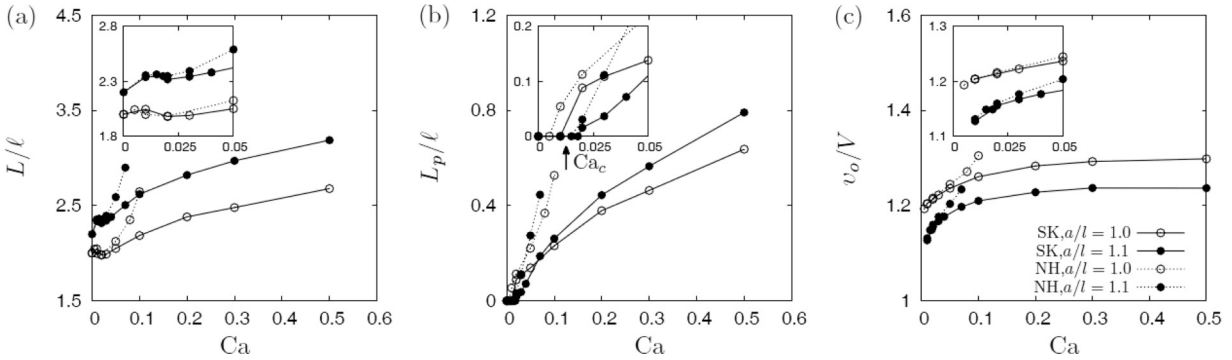

FIG. 5. Effect of Ca, a/ℓ and membrane law on the capsule total length L/ℓ, parachute depth L_p/ℓ, and center of mass velocity v_o/V.

of 4% on L/ℓ. The parachute depth is more difficult to measure with precision. For $L_p/\ell < 0.05$ we consider that there is no parachute and that we are close to the critical value Ca_c. For $0.05 < L_p/\ell < 0.1$, we take a tolerance of 50%. For $0.1 < L_p/\ell < 0.2$, we take a tolerance of 25% and for higher values the tolerance is 15%.

The size ratio is first calculated from a_{app}/ℓ, Ca and the corresponding database. For the first iteration, Ca is initialized with the mean value of the total range (which depends on the membrane constitutive law). The size ratio is then used to calculate two ranges of possible capillary numbers from the experimental values of L/ℓ and L_p/ℓ with their tolerances. If these two ranges intersect, we calculate and use the intersection mean value to process the next iteration of the algorithm until the mean value of Ca remains constant within 10^{-3} over two successive iterations. For each value of Ca in the intersection interval, we calculate the mean fluid velocity V from the capsule velocity v_o and the velocity ratio v_o/V of the database. Finally, we calculate the shear moduli that correspond to each Ca in the intersection interval by means of Eq. (3). This procedure is executed for 5 values of a_{app}/ℓ (a_{app}/ℓ, $a_{\mathrm{app}}/\ell \pm 1\%$, and $a_{\mathrm{app}}/\ell \pm 2\%$) to take

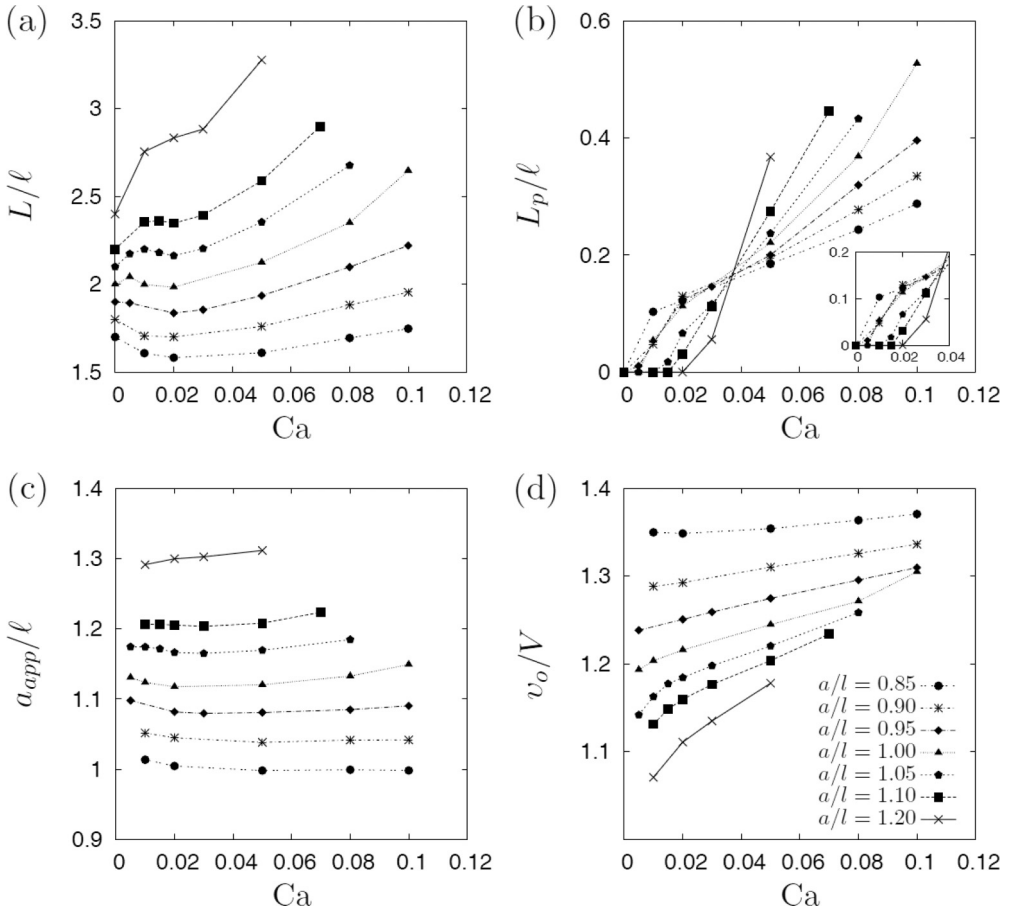

FIG. 6. Plots of the capsule total length L/ℓ, parachute depth L_p/ℓ, approximate radius a_{app}/ℓ, and velocity of mass center v_o/V obtained with the NH law.

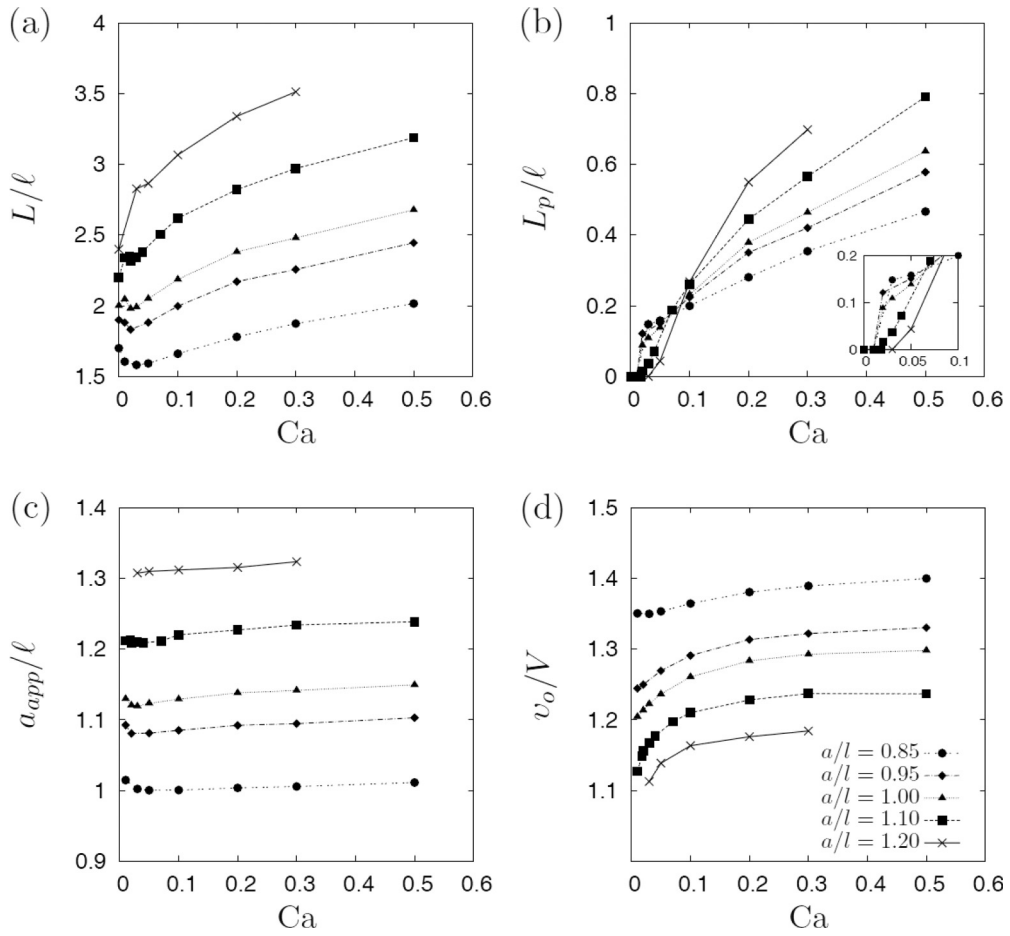

FIG. 7. Plots of the capsule total length L/ℓ, parachute depth L_p/ℓ, approximate radius a_{app}/ℓ, and velocity of mass center v_o/V obtained with the SK law ($C = 1$).

into account a relative uncertainty of about 2%. Then, we calculate the mean value of the shear modulus and the standard deviation.

IV. RESULTS AND DISCUSSION

A. Capsule deformation in a square-section channel

Typical profiles of capsules mildly to highly deformed in a square-section channel are shown in Fig. 8. Capsules (a) and (c) have almost the same apparent size, which corresponds to an actual size ratio of order $a/\ell = 0.9$ (Fig. 6 or 7). However capsule (c) has a higher velocity than capsule (a). As a consequence capsule (c) is more deformed than capsule (a) and has a deeper parachute. The same phenomenon is observed for capsules (e) and (g), which have the same apparent size corresponding to an actual size ratio of order $a/\ell = 1.05 \sim 1.1$. Being the fastest one, capsule (g) is the most deformed with the deepest parachute.

B. Determination of membrane properties

As an example, we first apply the inverse analysis algorithm with either the NH or the SK law, to a typical capsule which is smaller than the pore [profile (d) of Fig. 8]. We find $a/\ell = 0.9$ in both cases, Ca $= 0.08$ for the NH law capsule and Ca $= 0.17$ for the SK law one. We then compute exactly the equilibrium-deformed profiles corresponding to these two cases and compare them with the experimental profiles in Fig. 9(a). We note that the deformed profile of a small capsule can be well fitted with either the NH or the SK law. However, the capillary number for the SK capsule is about twice that for the NH capsule, due to the strain-hardening property of the SK membrane, which requires higher loads to reach the same deformation as the NH one. The process is repeated for a capsule that is larger than the pore [profile (f) of Fig. 8]. We find two slightly different values of the initial radius $a/\ell = 1.1$ for the NH law and $a/\ell = 1.09$ for the SK law. The values of Ca are both small and of the same order, as should be expected, since for small deformation the two laws are equivalent. Computing the deformed profiles corresponding to the couples of values of a/ℓ and Ca with either the NH or the SK law, we can again fit them well to the experimental ones as shown in Fig. 9(b).

We then proceed to analyze a population of 18 capsules of different initial sizes, flowing through the square-section capillary tube at different flow rates. We use the inverse analysis algorithm to deduce, for each capsule, the mean value of the shear elastic modulus of the membrane G_s. We define

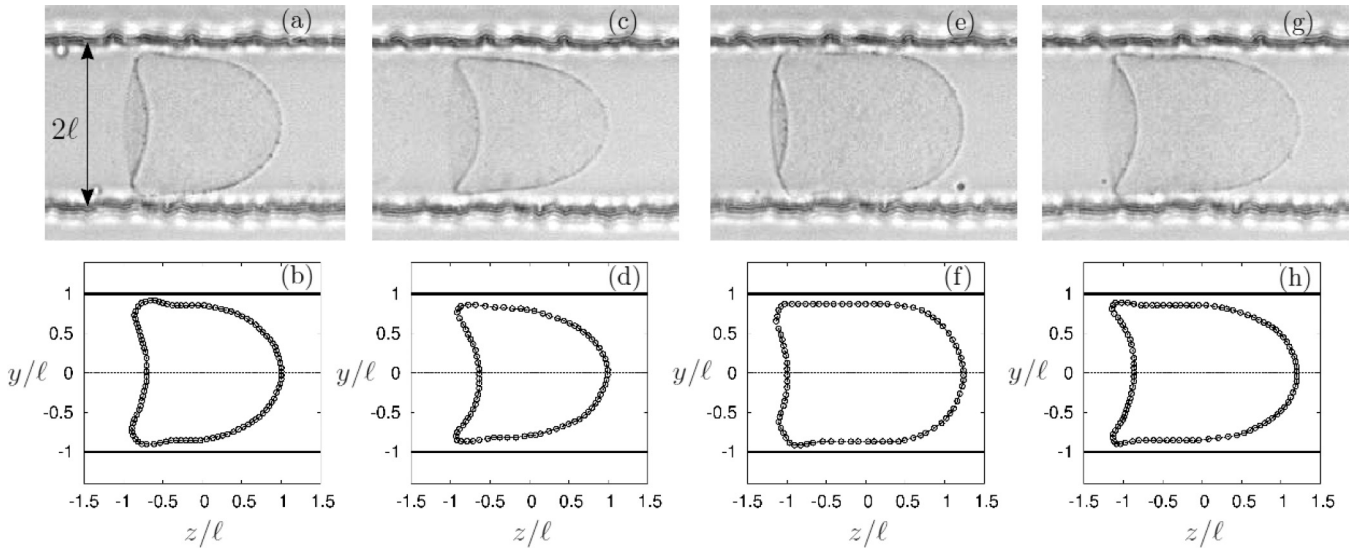

FIG. 8. Experimental images and corresponding extracted deformed profiles. The top row images are the original experimental images, while the bottom row figures are the corresponding extracted profiles. (a–b) $a_{\text{app}}/\ell = 1.08, v_o = 3.0$ mm/s; (c–d) $a_{\text{app}}/\ell = 1.05, v_o = 7.3$ mm/s; (e–f) $a_{\text{app}}/\ell = 1.2, v_o = 1.4$ mm/s; (g–h) $a_{\text{app}}/\ell = 1.16, v_o = 3.4$ mm/s.

the mean capsule elongation Λ

$$\Lambda = P/2\pi a \tag{14}$$

where P is the perimeter of the deformed capsule profile. It is then convenient to plot the values of G_s in terms of Λ rather than the size ratio. As shown in Fig. 10, when we assume a NH law for the membrane, we find a constant value of the shear modulus $G_s = 0.036 \pm 0.006$ N/m for a mean elongation ranging from 1 to 1.25 (which corresponds to a fairly large deformation!).

If we assume an SK law for the membrane, the value of G_s for small deformation ($\Lambda \leqslant 1.03$) is of the same order as the one obtained for the NH law. However, as the profile deformation increases, the corresponding values of G_s decrease by a factor three. This is a consequence of the strain-hardening property of the SK law. The fact that we cannot find a constant value for the shear modulus of the SK law for all deformation levels indicates that the membrane of ovalbumin capsules is not strain-hardening, but rather strain-softening as modeled by the NH law.

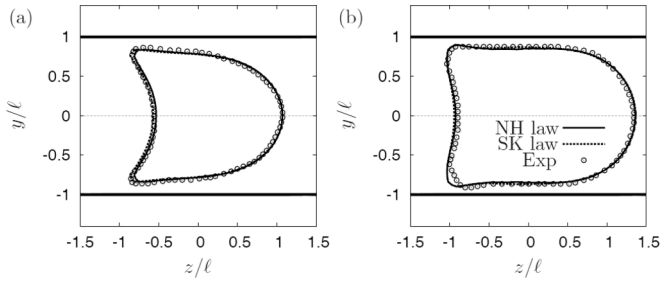

FIG. 9. Superposition of experimental and numerical capsule profiles in square-section microfluidic channel. The numerical profiles are obtained with the NH law or with the SK (C = 1.0) law. (a) NH law (Ca = 0.08, $a/\ell = 0.90$) and SK law (Ca = 0.17, $a/\ell = 0.90$); (b) NH law (Ca = 0.03, $a/\ell = 1.10$), and SK law (Ca = 0.05, $a/\ell = 1.09$).

V. DISCUSSION

The objective of this work was to determine plausible elastic properties for the membrane of capsules. We have chosen two simple constitutive laws with the *same* small deformation behavior, but with either strain-softening or strain-hardening properties under large strain. The use of the neo-Hookean law as the strain-softening one means that we have arbitrarily fixed the area dilation to shear modulus ratio to $K_s/G_s = 3$. For the strain-hardening law, we could have used values of C smaller than unity, which would have lowered the strain-hardening feature of the law (without eliminating it) and might have led to values of G_s less dependent on the deformation. However, using $C < 1$ would have made the comparison with NH law less meaningful as the small deformation parameters would have been different.

We note that there is some dispersion of the results in Fig 10. The dispersion is larger for the NH law than for the SK one. This is due to the fact that, when we use the NH law, the

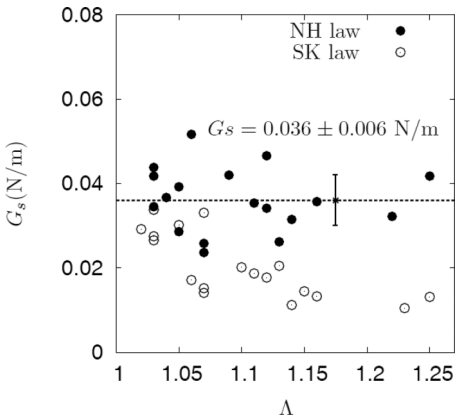

FIG. 10. Membrane shear modulus G_s as a function of capsule mean deformation Λ. Dashed line: average value of G_s determined with the NH law.

capillary number is small and the geometrical parameters L and L_p vary nonlinearly with Ca. When we use the SK law, the values of Ca are larger and the variation of L and L_p with Ca is almost linear.

Another question is linked to the fact that the channel we used is not perfectly square (as is usually the case with PDMS channels). Of course, we could have run the model with the exact dimensions of the channel, but we decided instead to provide general charts for the flow in square channels and use them to analyze our results. As a check, we compare the surface shear modulus value presently determined ($G_s = 0.036 \pm 0.006$ N/m) with the one obtained by Chu *et al.* [9] ($G_s = 0.042 \pm 0.016$ N/m). The ovalbumin capsules were prepared under the same conditions but they were flowed in a 50 μm glass capillary tube. The two mean values of G_s fall in the same range within experimental errors.

The reason why the ovalbumin membrane seems to be strain-softening is probably due to the conformation of the albumin molecule at the interface. For a small reticulation time of 5 min, the density of covalent links between the protein molecules is low and the protein chains are loosely linked. This may explain why the membrane is easily deformable, as described by an NH law. It has not been possible to obtain deformations larger than 25%, so that we do not know for what deformation the membrane breaks.

VI. CONCLUSION

We show here that it is possible to infer plausible mechanical properties of an artificial capsule membrane from experiments, where the capsule has to deform to flow inside a small square-section pore with cross dimensions of the same order as those of the capsule. The method is based on the coupling of experimental observations with a rigorous mechanical model of the system. It also implies a strong hypothesis on the value of the area dilation to shear modulus ratio, which is assumed to be $K_s/G_s = 3$. The method works well if the deformation of the capsule is large enough. Indeed, for a small deformation, it is not possible to distinguish between different laws and there is some dispersion in the results. Thus, it is best to use a pore, such that the size ratio of the capsules is of order unity. Small capsules ($a/\ell \leqslant 0.8$) have to be flowed quickly to be deformed with concomitant difficulties of observation leading to profile fuzziness. In order to reach large deformation, while keeping the capsule velocity moderate, a high-viscosity suspending liquid is necessary. But the price to pay is that the high-viscous-pressure drop inside the microchannel may lead to the destruction of the connections. The advantage of using a square-section channel rather than a cylindrical one is linked to the easy fabrication of microfluidic tubes of any size and to the easy connection with the propulsion device. Furthermore, this system can be built in a microfluidic fabrication device to monitor the properties of the capsules *in situ* [21]. We note that it is even possible to infer the large deformation behavior of the membrane, at least decide whether it is strain-softening or -hardening.

ACKNOWLEDGMENTS

This work was supported by the Conseil Régional de Picardie (MODCAP grant), by the French Agence Nationale de la Recherche (CAPSHYDR grant ANR-11-BS09-013), and by the French Ministère de la Recherche (Pilcam2 grant). X.-Q. Hu acknowledged support from the China Scholarship Council through a Ph.D. scholarship. The capsules were provided by Dr. Florence Edwards-Lévy, Institut de Chimie Moléculaire de Reims (UMR CNRS 7312), Université de Reims Champagne-Ardenne, Reims, France.

[1] D. Barthès-Biesel, Curr. Opin. Colloid Interface Sci. **16**, 3 (2011).
[2] M. Carin, D. Barthès-Biesel, F. Edwards-Lévy, C. Postel, and D. Andrei, Biotechnol. Bioeng. **82**, 207 (2003).
[3] K. S. Chang and W. L. Olbricht, J. Fluid Mech. **250**, 609 (1993).
[4] M. Husmann, H. Rehage, E. Dhenin, and D. Barthès-Biesel, Int. J. Colloid Interface Sci. **282**, 109 (2005).
[5] C. A. Putman and K. O. Van der Werf, Biophysical J. **67**, 1749 (1994).
[6] A. Fery and R. Weinkamer, Polymer **48**, 7221 (2007).
[7] R. M. Hochmuth, J. Biomechanics **33**, 15 (2000).
[8] Y. Lefebvre, E. Leclerc, D. Barthès-Biesel, J. Walter, and F. Edwards-Lévy, Phys. Fluids **20**, 123102 (2008).
[9] T. X. Chu, A.-V. Salsac, E. Leclerc, D. Barthès-Biesel, H. Wurtz, and F. Edwards-Lévy, Int. J. Colloid Interface Sci. **355**, 81 (2011).
[10] S. Kuriakose and P. Dimitrakopoulos, Phys. Rev. E **84**, 011906 (2011).
[11] R. Skalak, A. Tozeren, R. P. Zarda, and S. Chien, Biophys. J. **13**, 245 (1973).
[12] Y. Lefebvre and D. Barthès-Biesel, J. Fluid Mech. **589**, 157 (2007).
[13] J. Walter, A.-V. Salsac, D. Barthès-Biesel, and P. Le Tallec, Int. J. Numerical Methods Eng. **83**, 829 (2010).
[14] X.-Q. Hu, A.-V. Salsac, and D. Barthès-Biesel, J. Fluid Mech. **705**, 176 (2012).
[15] F. Edwards-Lévy, M. C. Andry, and M. C. Lévy, Int. J. Pharmaceutics **96**, 85 (1993).
[16] J. C. McDonald and G. M. Whitesides, Acc. Chem. Res. **35**, 491 (2002).
[17] G. S. Fiorini and D. T. Chiu, BioTechniques **38**, 429 (2005).
[18] J. B. Segur and H. E. Oberstar, Ind. Eng. Chem. **43**, 5 (1951).
[19] C. Pozrikidis, Annals Biomed. Eng. **33**, 165 (2005).
[20] D. Barthès-Biesel, A. Diaz, and E. Dhenin, J. Fluid Mech. **460**, 211 (2002).
[21] T. X. Chu, A.-V. Salsac, D. Barthès-Biesel, L. Griscom, F. Edwards-Lévy, and E. Leclerc, Microfluidics Nanofluidics **14**, 309 (2013).